ZPh-110
Physics Section

EXPERIMENTAL DETERMINATION OF THE SLOW *NO* DECOMPOSITION REGIME AROUND 3000°K BEHIND SHOCK WAVES

C. B. Ludwig

K. G. P. Sulzmann

P. S. Hrbacek

June 30, 1961

This work was supported by the Army Rocket and Guided Missile Agency Under Contract DA-04-495-ORD-3112, ARPA Order No. 39-52, Task 2

GENERAL DYNAMICS | CONVAIR

ZPh-110
Physics Section

EXPERIMENTAL DETERMINATION OF THE SLOW *NO* DECOMPOSITION REGIME AROUND 3000°K BEHIND SHOCK WAVES

C. B. Ludwig

K. G. P. Sulzmann

P. S. Hrbacek

June 30, 1961

This work was supported by the Army Rocket and Guided Missile Agency Under Contract DA-04-495-ORD-3112, ARPA Order No. 39-59, Task 2

GENERAL DYNAMICS | CONVAIR

CONTENTS

ILLUSTRATIONS

ILLUSTRATIONS - (Cont'd)

EXPERIMENTAL DETERMINATION OF THE SLOW *NO* DECOMPOSITION REGIME AROUND 3000°K BEHIND SHOCK WAVES

C. B. Ludwig
K. G. P. Sulzmann
P. S. Hrbacek

ABSTRACT

The decomposition of nitric oxide between 2250 and 3450°K has been studied in shock tube experiments. The emitted infrared radiation of the fundamental band system of NO has been used to determine the time duration of the slow decomposition regime of NO behind shock waves in pure NO. It is found that the temperature dependency of the duration is in good agreement with the theoretical model we have described previously.

INTRODUCTION

The experiments which led to the determination of the rate constant in the exchange reaction $NO + O \rightarrow N + O_2$ around 3000°K will be described. These experiments were conducted in a 3-in. shock tube, in which undiluted nitric oxide gas at 10 mm Hg and at approximately 300°K was subjected to helium driven shock waves of about M = 7. The relative concentration history of the heated NO was followed by its infrared emission from the fundamental band systems. A slit system was used to observe the radiation from a 3-mm-wide gas slab (at the opposite shock tube wall) in the direction normal to the gas flow.

It has been established from our observations and also from other publications[1,2] that the radiation intensity of NO behind shock waves decreases very slowly over some period of time (Regime I), the length of which depends on the temperature of the gas. Regime I is followed by a second regime during which the radiation intensity decreases rapidly. It was found analytically[3] that Regime I of the radiation history could be ascribed to the slow decomposition of NO and, further, that the length of this regime was a sensitive function of the rate constant of the reaction mentioned above as well as of the temperature. In our experiments, the duration of Regime I as function of the shock temperature has been determined.

ASSUMPTIONS

To interpret the emitted radiation intensity of NO as being proportional to the concentration of NO, the following assumptions must be made.

1. The translational and internal degrees of freedom are equilibrated before the chemical reactions take place, and
2. Variables of state, on which the radiation will depend, do not change appreciably during the time the measurements are made.

The first assumption seems well satisfied in view of recent measurements.[4] It has been shown that the relaxation time for NO is short ($< 1\ \mu$sec) not only for the translational and rotational, but also for the vibrational equilibration at our test conditions. The vibrational transition probability P_{1-0} was measured[4] at 1000°K and found to be approximately 3×10^{-3}. By assuming $P_{1-0} = 10^{-2}$ for 3000°K, we obtain a relaxation time (laboratory system) of

$$t_L = \frac{2.86}{p_S \left(\rho_o/\rho_S\right)^2 T_o^{1/2} P_{1-0}} \sim 1\ \mu\text{sec}$$

for p_s = 650 mm Hg, ρ_s/ρ_o = 4 and T_o = 300 °K.

It is, therefore, reasonable to adopt a simplified model which accounts for the chemical relaxation only, after the translational, rotational, and vibrational equilibrium with temperature T_s has been reached. We can also assume, that in the temperature range up to 3500 °K, processes involving electronic transitions and ionization are negligible. This assumption is based upon equilibrium calculations made by Gilmore.[5] It can be shown that only one NO molecule in one million is excited from the $(X^2\pi)$ state to the $(A^2\Sigma^{\pm})$ state at 5000 °K.* The excitation of NO^+ to the 3π state is 1 particle in 100,000 at this temperature, whereby the ratio of

$$\left(\frac{NO^+}{NO}\right)_{3000\,^\circ K} \approx 3.10^{-7}$$

at 1 atm. The other species involved exhibit similar small ratios with the exception of O_2

$$\left.\frac{O_2\,(a^1\Delta^8_g)}{O_2\,(X^3\Sigma^9_g)}\right|_{3000\,^\circ K} \lesssim 3\% .$$

Although all of these ratios of electronically excited to unexcited species seem to be rather small and, therefore, were neglected in our considerations, it is still conceivable that they could influence to some measure the reaction scheme in the transition zone. However, no attempt was made to assess this influence. It may be noted that the relaxation processes involving electronic transitions also were neglected by others,[6,7] even in temperature ranges much higher than ours.

---

*Gilmore does not list any value below 5000 °K for N_2, NO, and NO^+.

The second assumption above is necessary because the emitted radiation intensity is the only experimental parameter from which the NO concentration may be determined. It is found that for a constant number of NO molecules in the harmonic oscillator and transparent gas approximation, the total infrared emissivity changes 5% for each 100°K temperature change (between 2000 and 3500°K). Therefore, the second assumption is only satisfied for Regime I. Calculations show[3] the temperature T and the density ρ during RegimeI to change only by 2%. On the other hand, the chemical equilibrium temperature T_e and density ρ_e may deviate from the shock temperature T_S and density ρ_S by as much as 30 and 50%, respectively.

The shock temperature T_S as the primary parameter and the equilibrium temperature T_e were calculated from the shock front velocity by using the Los Alamos Equilibrium Code.* The shock temperature T_S and initial density ρ_S were computed for frozen chemistry by assuming transiational, rotational, and vibrational equilibrium.

These calculations were used to plot the Hugoniot curves p/p_o versus ρ_o/ρ (Figure 1), the temperatures T_S and T_e and the density ratios versus shock velocity (Figure 2), and equilibrium concentrations of the species involved versus temperature T_e (Figure 3).

EXPERIMENTAL TOOL

The Shock Tube

The experiments have been carried out in a 3-in. stainless steel tube with a polished internal surface. A description of the physical structure of this tube

---

*Courtesy of Dr. R. Duff, Los Alamos Scientific Laboratory, Los Alamos, New Mexico.

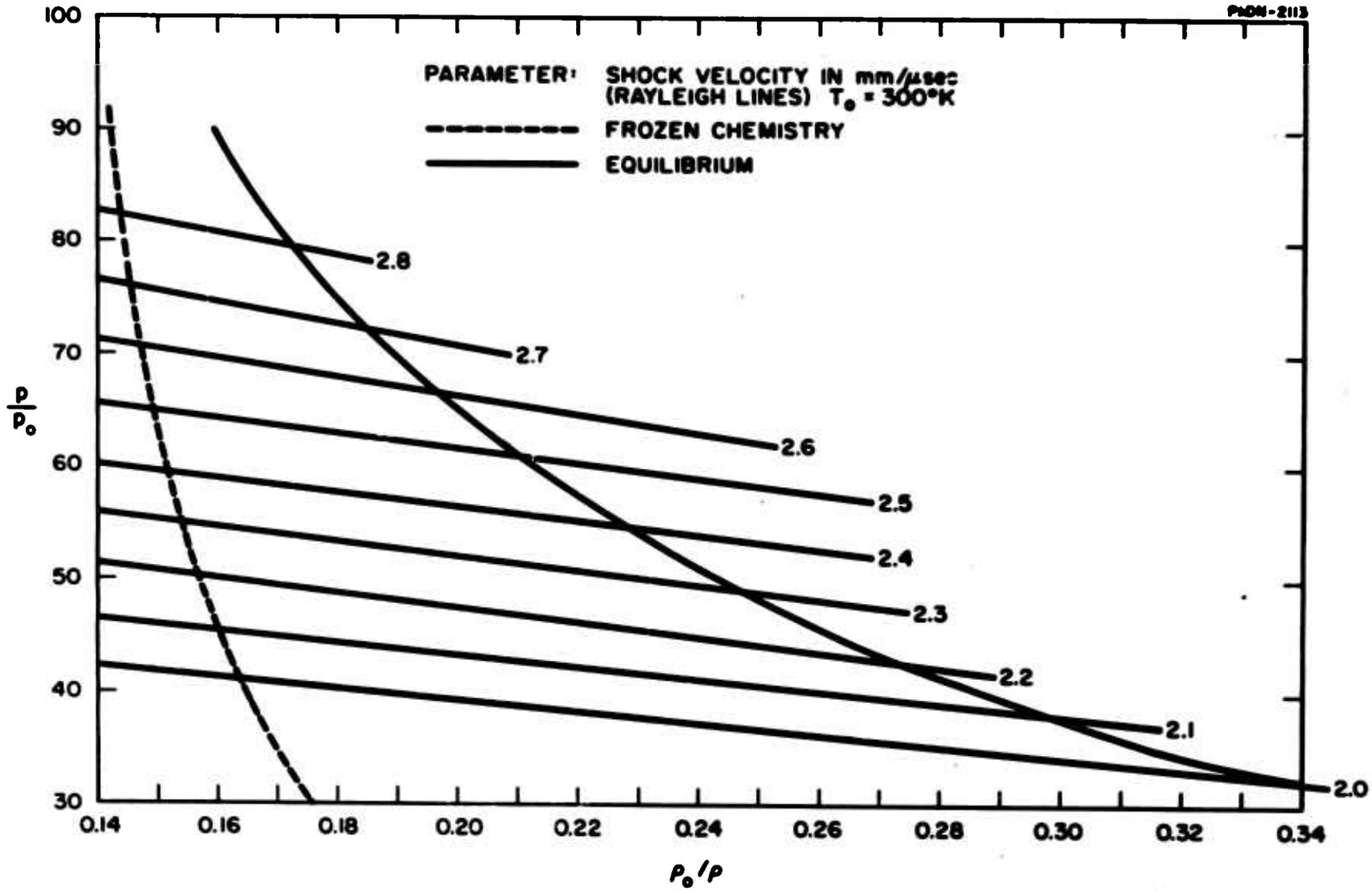

FIGURE 1 HUGONIOT CURVES p/p_o VS ρ_o/ρ

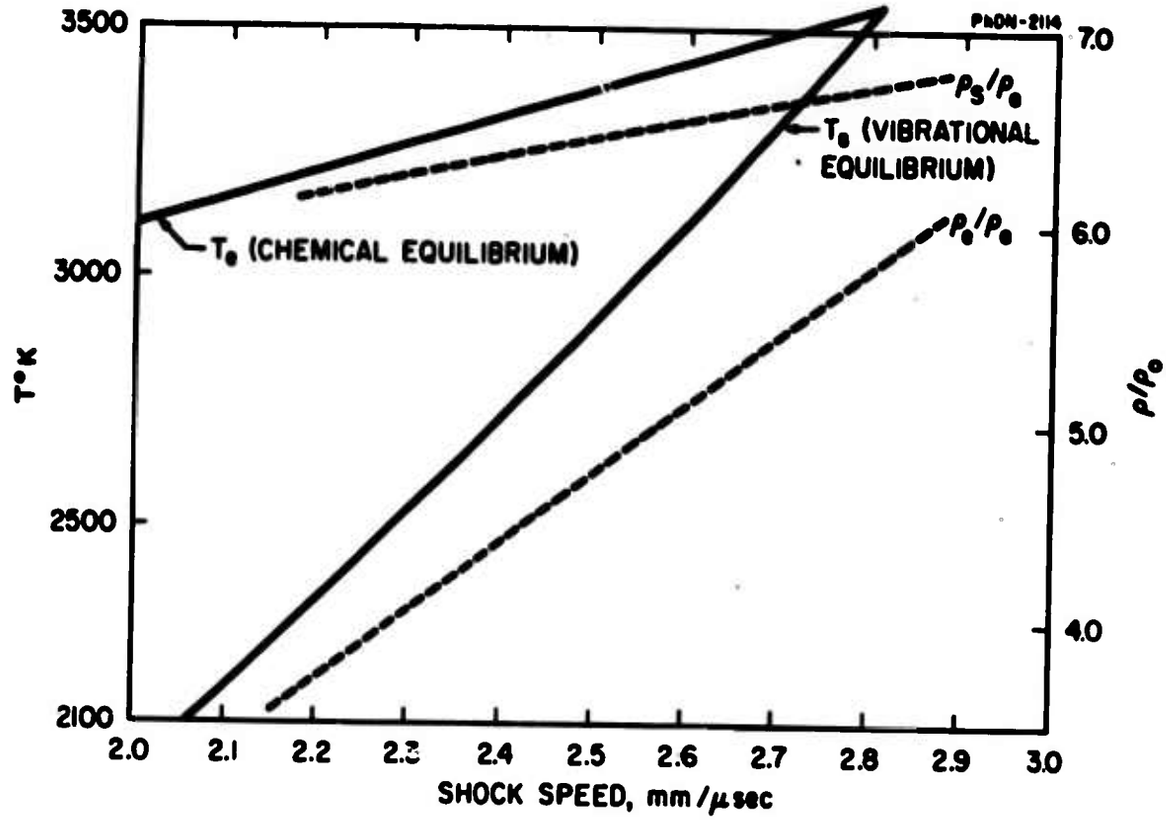

FIGURE 2 TEMPERATURE AND DENSITY RATIO VS SHOCK VELOCITY

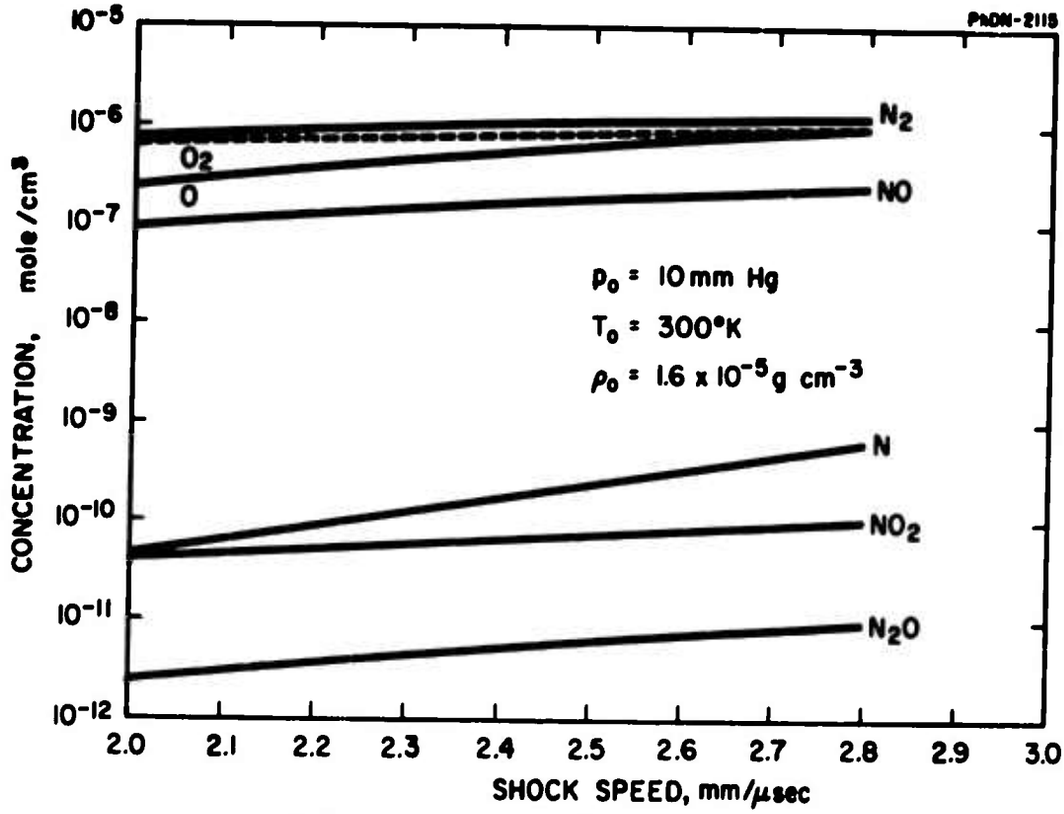

FIGURE 3 CONCENTRATIONS VS TEMPERATURE

has been given earlier[8] so that we can restrict our present discussion to the improved vacuum system and the control of the contamination level.

The experimental setup of the tube is shown in Figures 4 and 5. A detailed schematic diagram of the vacuum system is shown in Figure 6. The 4-ft driver (Figure 7) separated from the shock tube by a copper diaphragm (with X-inscription), was evacuated by a small roughing pump to about 100μ Hg before helium was admitted. The 25-ft-long test section, separated from the expansion tank by a 1-mil brass shim shock diaphragm,* was first roughed down to 5μ with a mechanical pump and then evacuated by two 4-in. oil diffusion pumps to 2×10^{-5} mm Hg. The three pumps were connected to the shock tube by 2-in. copper tubing. Two different valves are used with each pump: The first valve is incorporated into the shock tube and is flush with the inside diameter in the "closed" position. Since this valve cannot hold high vacuum, the second, a gate valve, is used to separate the tube from the pump. Both diffusion pumps have liquid nitrogen traps. The expansion tank was roughed down to approximately 100μ Hg.

The fore vacuum in the shock tube was measured by a Pirani gauge (Autovac) and the high vacuum by two Philips ionization gauges. All gauges were repeatedly calibrated against a McLeod gauge. The pressure of the test gas was measured by an Octoil-S-Manometer (U-tube). The density ratio of Octoil-S to mercury was determined by a McLeod gauge and is 14.9 ± 0.05 at room temperature. The initial temperature T_o of the test gas was assumed to be room temperature, which was confirmed by a thermocouple placed inside the tube.

---

*Mylar was previously used but has been discarded because partial pyrolysis occurred after rupture with subsequent development of contaminating fumes.

PhDN-2116

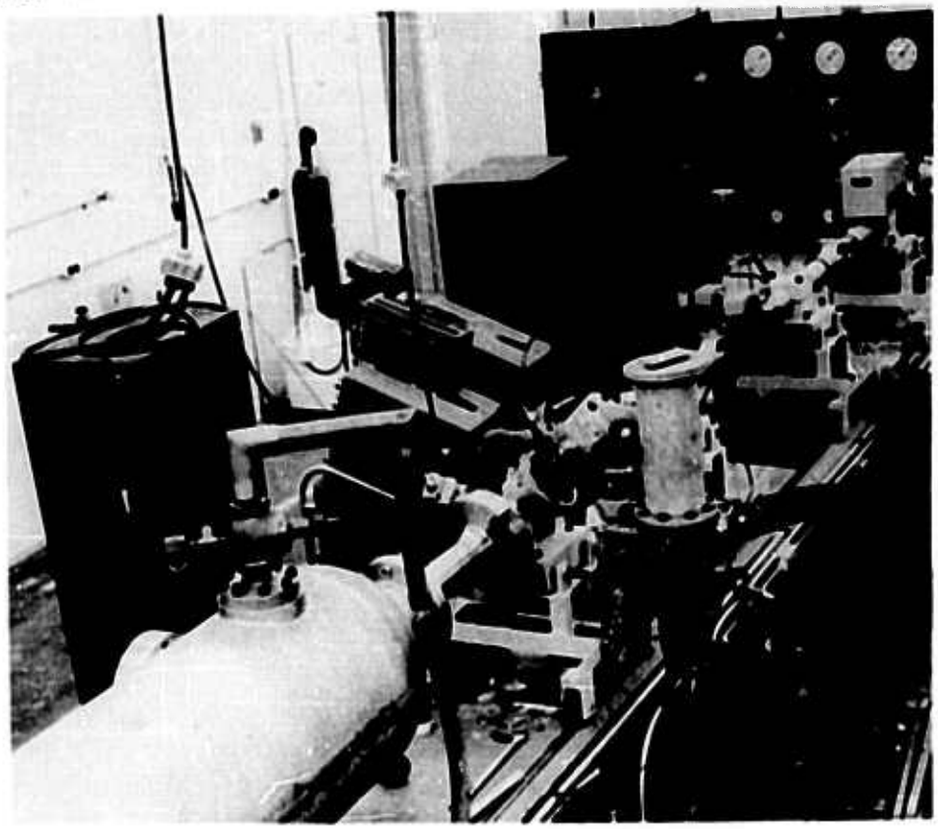

FIGURE 4 SHOCK TUBE

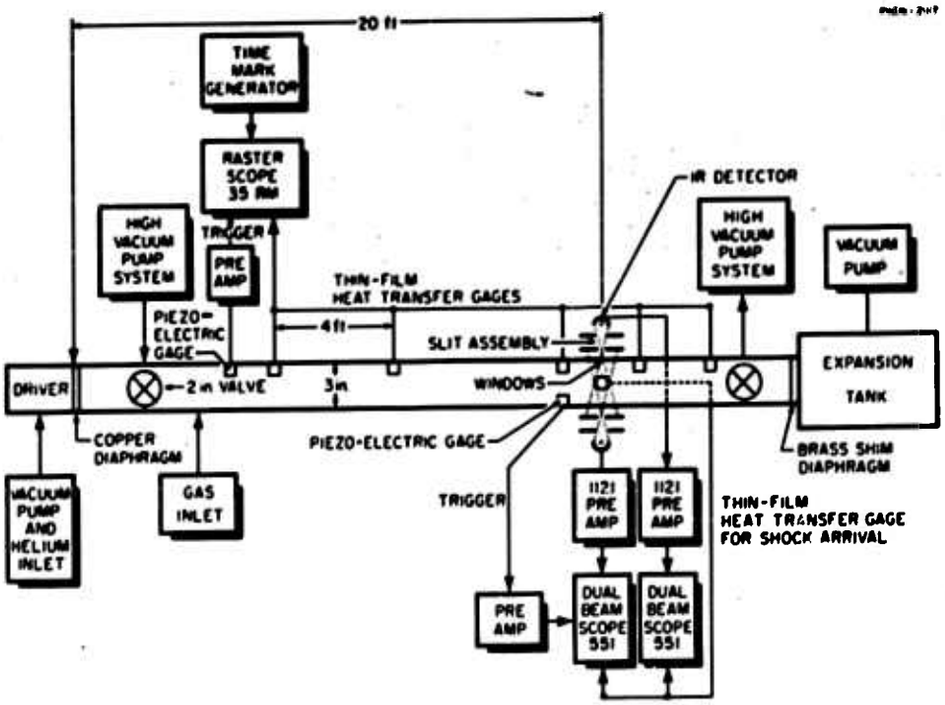

FIGURE 5 SHOCK TUBE DIAGRAM

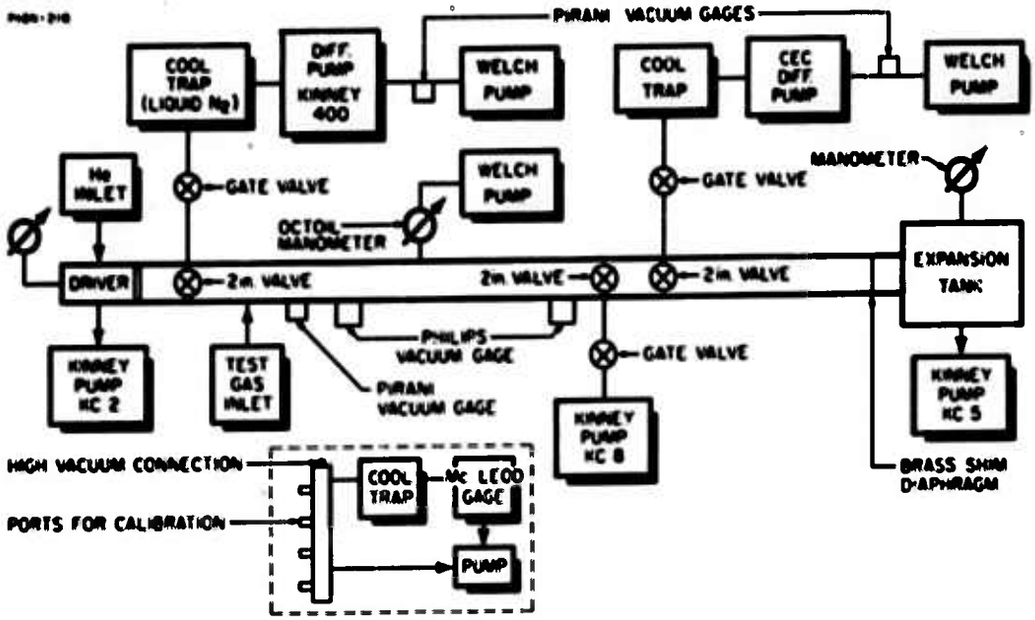

FIGURE 6 VACUUM SYSTEM

PhDN-2119

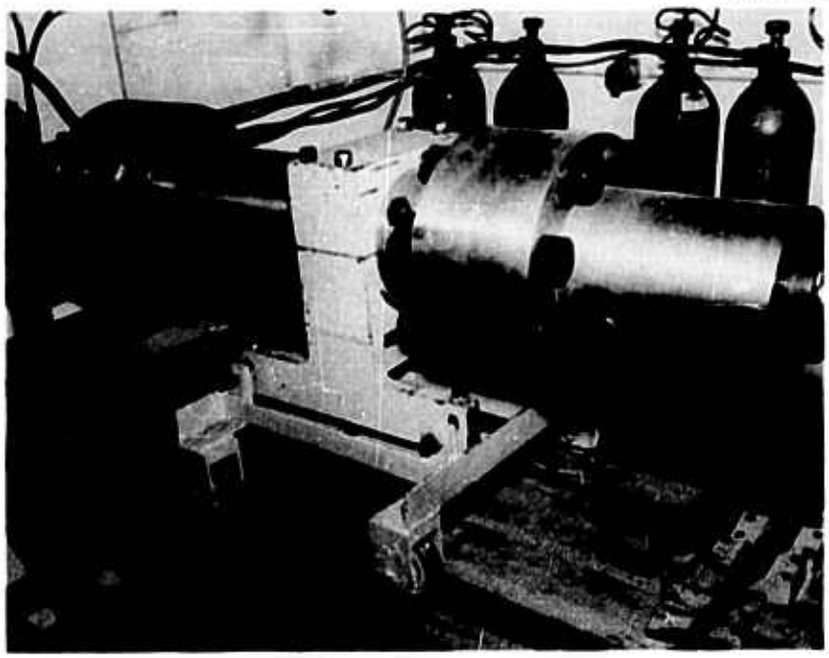

FIGURE 7 DRIVER SECTION

Two main sources of contamination were impurities in the test gas and residual gases at the shock tube walls. The manufacturer's (Matheson) values for the impurities of the NO test gas are 0.557% N_2 and 0.279% NO_2. However, our analysis with a mass spectrometer showed ~ 0.7% N_2 and ~ 0.3% N_2O. This analysis was confirmed qualitatively by an infrared absorption spectrum taken from a 10-m gas cell. This amount of contamination influenced our experimental results by not more than 30%, which is within the limits of the other experimental errors. The contamination level caused by the residual gases in the shock tube was well below that of the test gas. The pressure equilibration after closing the diffusion pump valves resulted in a pressure of 10^{-4} mm Hg; the leak rate at this pressure was 0.1μ/min. By assuming 2 min. for filling the tube with 10 mm Hg of NO, we had 0.003% contamination in the tube. On the other hand, it was found that repeated shocks through NO resulted in tube wall contamination which could not be removed by pumping alone. This contamination became apparent by infrared emission from shock-heated argon. After several argon shocks this radiation disappeared, therefore, it was decided to "clean" the tube after each NO test run with an argon run. In each of these argon runs, no radiation in the 2 to 6μ region was observed even after increasing the amplification 10 times.

Velocity Measurement

The velocity measurements were made with five heat-transfer gauges. These gauges were obtained by sputtering a 1/2-mm-wide and 6-mm-long platinum strip on polished glass. These strips had a d-c resistance of ~ 100 to 200 ohms. After sputtering, the platinum strips were baked for 30 min. at 1400°F which lowered the resistance to ~ 100 to 200 ohms. Two wires were attached at both ends of the strips with conducting epoxy (Emerson). The glass plugs were then inserted in steel plugs by apiezon wax. A discontinuity existed of about 0.5 mm between the flat glass and the curved inside diameter of the

tube. The electronic and geometrical arrangement of the gauges in the tube is shown in Figure 8. The potentiometer R_p was set equal to the resistance of the gauge to obtain maximum voltage output (about 20 mv, Appendix I). The rise times were found to be less than 1 μ sec. The signals of the five gauges were given on a Tektronix 35RM scope, which was modified to produce a raster sweep of variable length. (The fly-back time was equal to the sweep time.) The beam intensity was modulated by 100, 10, and 1 μ sec time marks from a Tektronix time mark generator 180. It was found that a very clear picture was obtained by inverting the polarity of the time marks by a Tektronix pre-amplifier 121. (A representative oscillogram is given in Figure 9.)

The raster scope was triggered by a Kistler miniature piezoelectric gauge, which was located 57 mm ahead of the first heat-transfer gauge. The output of ~ 5 mv was amplified roughly 10,000 times by a transistorized pre-amplifier which suppressed the negative signal.*

The reading accuracy of the signals on the oscillogram, determined by the rise time of the gauges and the time markings on the sweep, was ± 1 μ sec. This introduced an instrumental error in the velocity determination of ± 0.16 to ± 0.23% for the long distance of 1219.2 mm and of ± 1.2 to 1.6% for the shorter distance of 171.5 mm between the heat-transfer gauges. The two values given correspond to the limiting shock velocities of 2.0 and 2.8 mm/μ sec, respectively. In addition to the instrumental error, an uncertainty exists about the velocity at each point along the tube. This uncertainty is, of course, larger for longer distances between two gauges. This is the reason why we chose a short distance for our velocity determination, at the observation station, although our reading accuracy at this point is decreased by a factor of 10. An

---

*The schematic drawings of this amplifier were given to us by Dr. T. Jacobs (California Institute of Technology, Pasadena, California).

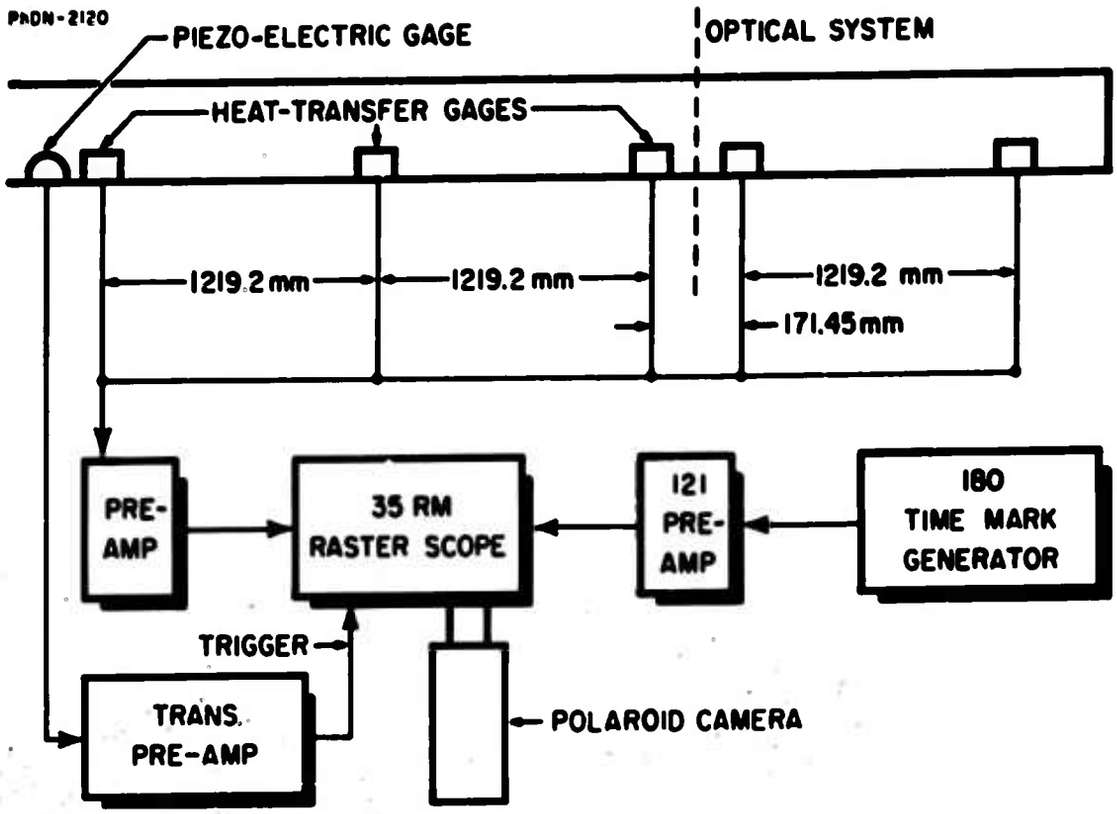

FIGURE 8 VELOCITY MEASUREMENTS

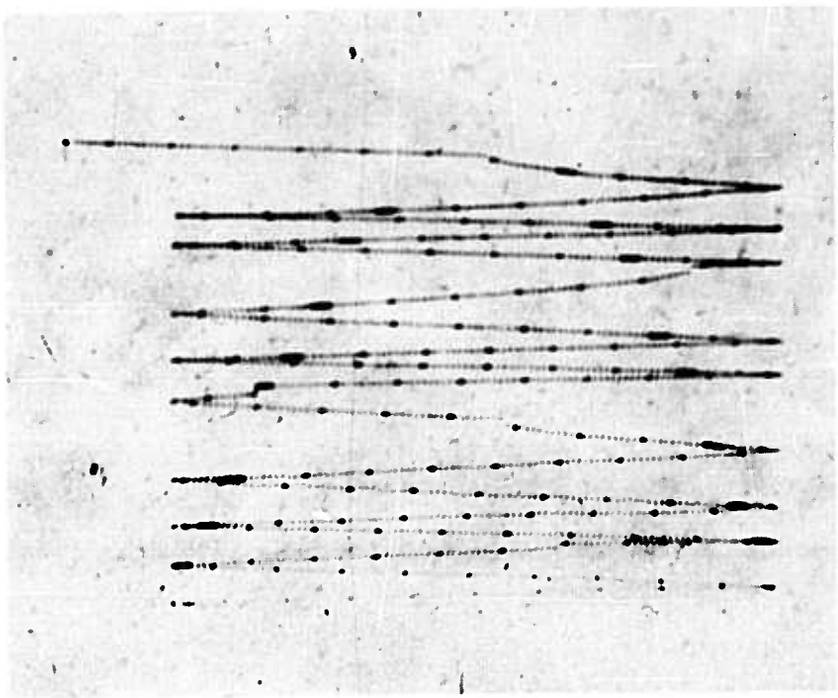

FIGURE 9 RASTER OSCILLOGRAM

attempt was made to increase the reading accuracy by using electronic counters with a resolution of 0.1 μsec. However, the stability of self-built trigger amplifiers was not good enough to ensure reproducible precision for this type of measurement.

If we plot our time readings in the usual x-t diagram (Figure 10), the shock wave propagation seems to be linear. However, deviations up to 10% from the linear behavior do exist. These deviations are shown in Figure 11; the average velocities between two adjacent pickups have been normalized to the mean velocity measured at the location of the optical detector. Accelerated, as well as monotonically attenuated (as observed in inert gases) shock waves have been obtained. This fact is attributed to the influence of the chemical reactions on the shock propagation.

Prior to the NO test runs, the response of the gauges was determined by 50 check runs. Three gauges were mounted at the same location for direct comparison of their response. No difference greater than 0.5 μsec was found between the original rise of any two gauges.

Optical System

To monitor the concentration profile of NO, the infrared radiation of the fundamental band region was used. Additional observations of the first overtone region of NO (curve c of Figure 13) showed, within the experimental error that the intensity histories of both regions were the same. Therefore, instead of recording the radiation from the first overtone region, the radiation from the gas over the entire spectral region was observed.

According to the spectroscopical constants of NO the fundamental band head is located at 4.95μ; the band continues to be rather strong up to 6μ. The spectral characteristics of the window material, filters, and detector were chosen so that most of the radiation in this region could be collected

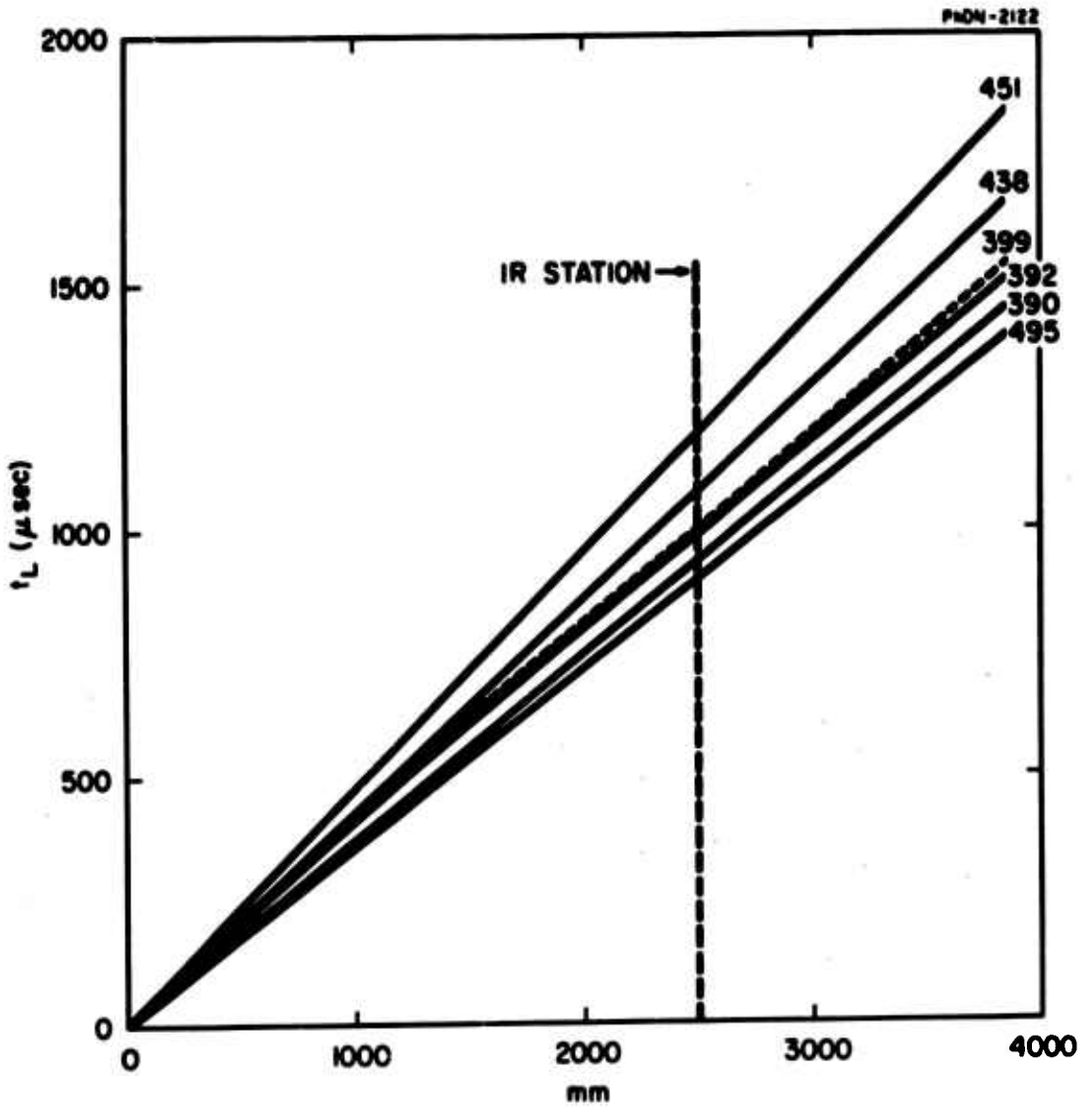

FIGURE 10 VELOCITY MEASUREMENTS, x VS t DIAGRAM FOR DIFFERENT SHOTS

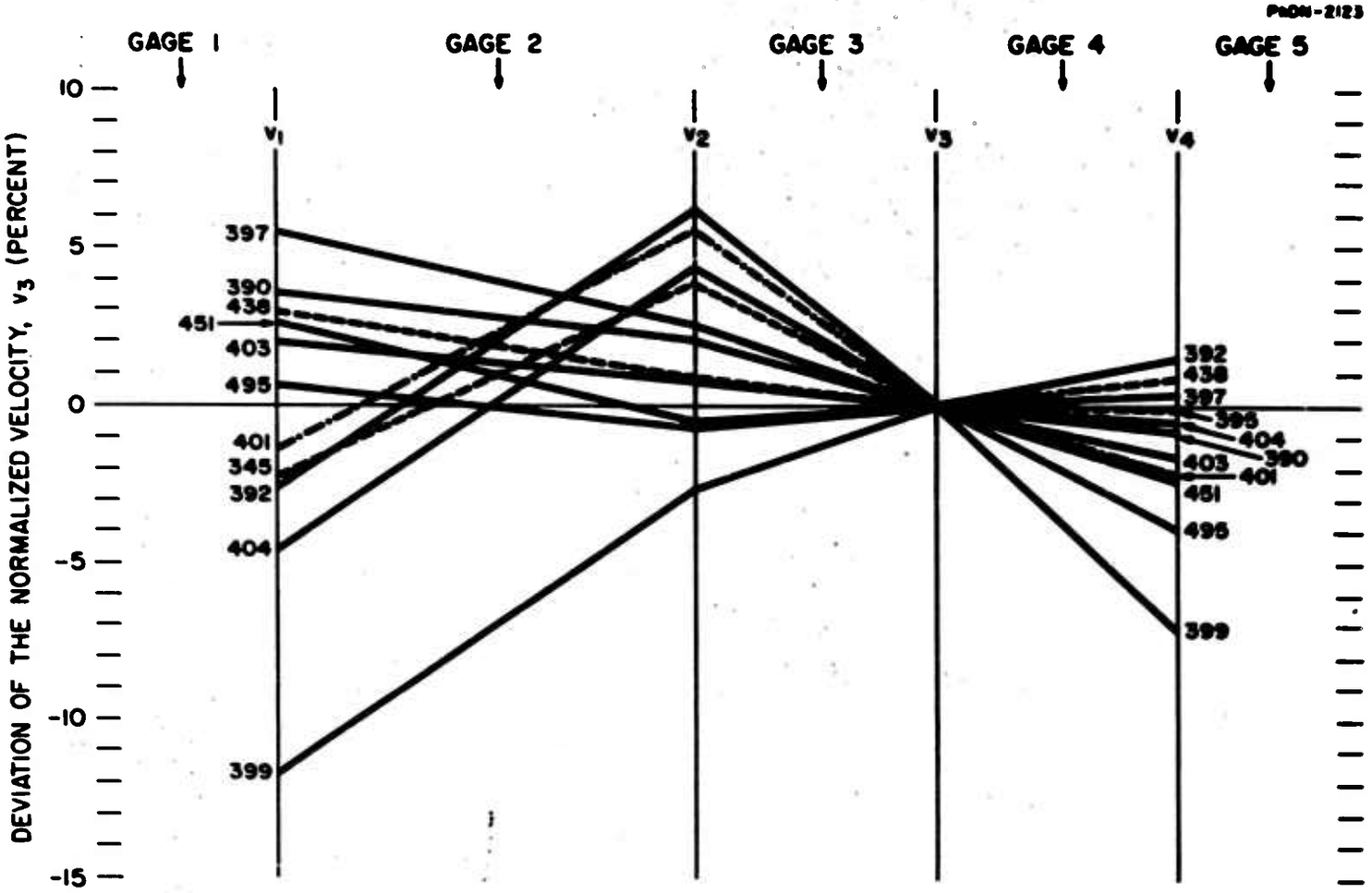

FIGURE 11 VELOCITY PROFILES FOR DIFFERENT SHOTS

(curve a of Figure 13). Detailed transmission curves of the window and filter, as obtained by a Beckmann monochromator, are given in Figures 12 and 13.

The optical system was set up as follows. A 0.6-cm-thick, flat surface, sapphire window was cemented in an instrument plug. The radiation energy from this window passes through a narrow 0.4-mm-wide and 6-mm-high slit and is reflected at a right angle by an aluminum mirror on to a second slit. This second slit has a 2 x 2 mm aperture through which the radiation passes on to the sensitive area (2 x 2 mm) of an indium-antimonide detector (Texas Instruments). The reflections inside the slit mirror housing are eliminated by large-diameter, threaded, and blackened bores (Figures 14 and 15). Internal reflections from the shock tube have been reduced by painting the walls black for 28 mm up- and downstream from the window. The slits have been arranged geometrically so that the radiation impinging on the detector is collected from a gas slab, which is 3 mm wide and 12 mm high at the opposite shock tube wall.

Since the In-Sb detector is a low-impedance, photo-voltaic device the voltage signal was fed directly into a pre-amplifier (Tektronix 1121) with an amplification factor of 100. The signal is then fed to the oscilloscope pre-amplifier. The liquid-nitrogen-cooled detector has an output of 80 mv for the background radiation of our experiments, which is compensated by a dry cell.

The dual-beam oscilloscope for the display of the radiation signal was triggered in the same way as the raster scope for the velocity measurement.

The second beam of this oscilloscope was used to record the arrival of the shock front at the window by a heat-transfer gauge. The location of this gauge and the optical axis of the window fall into the same plane perpendicular to the shock tube axis. The electronic equipment is shown in Figure 16.

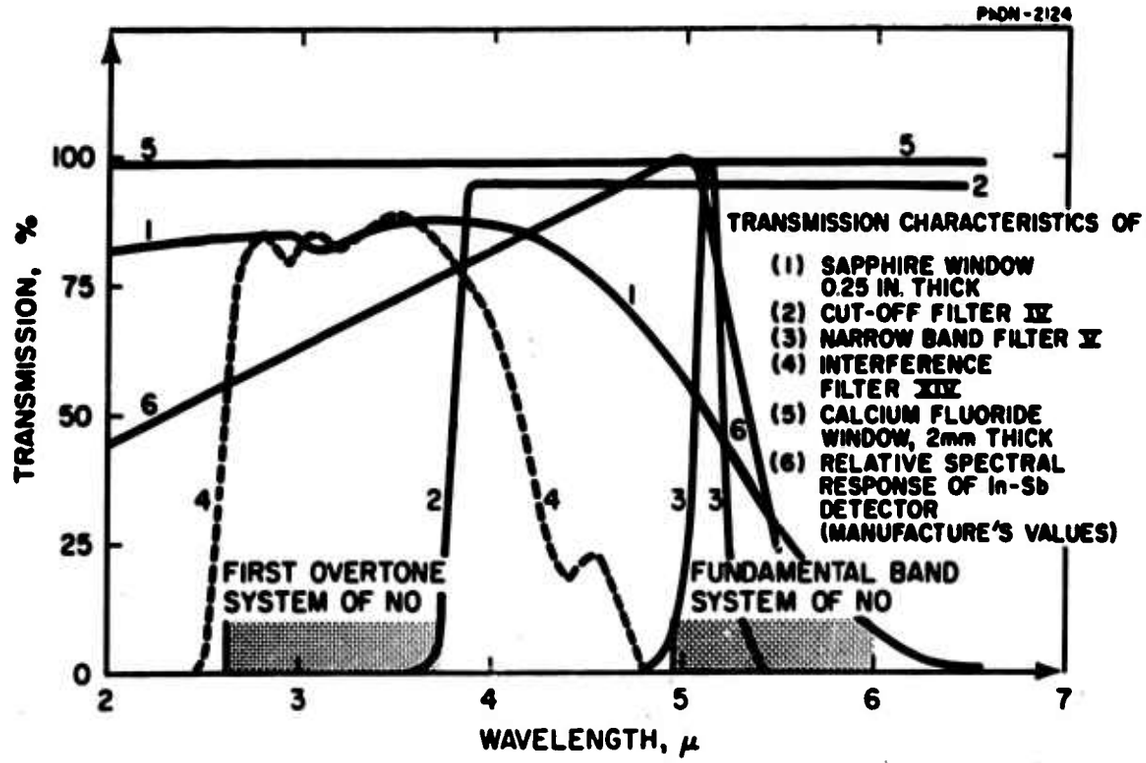

FIGURE 12 TRANSMISSION CHARACTERISTICS OF WINDOWS AND FILTERS

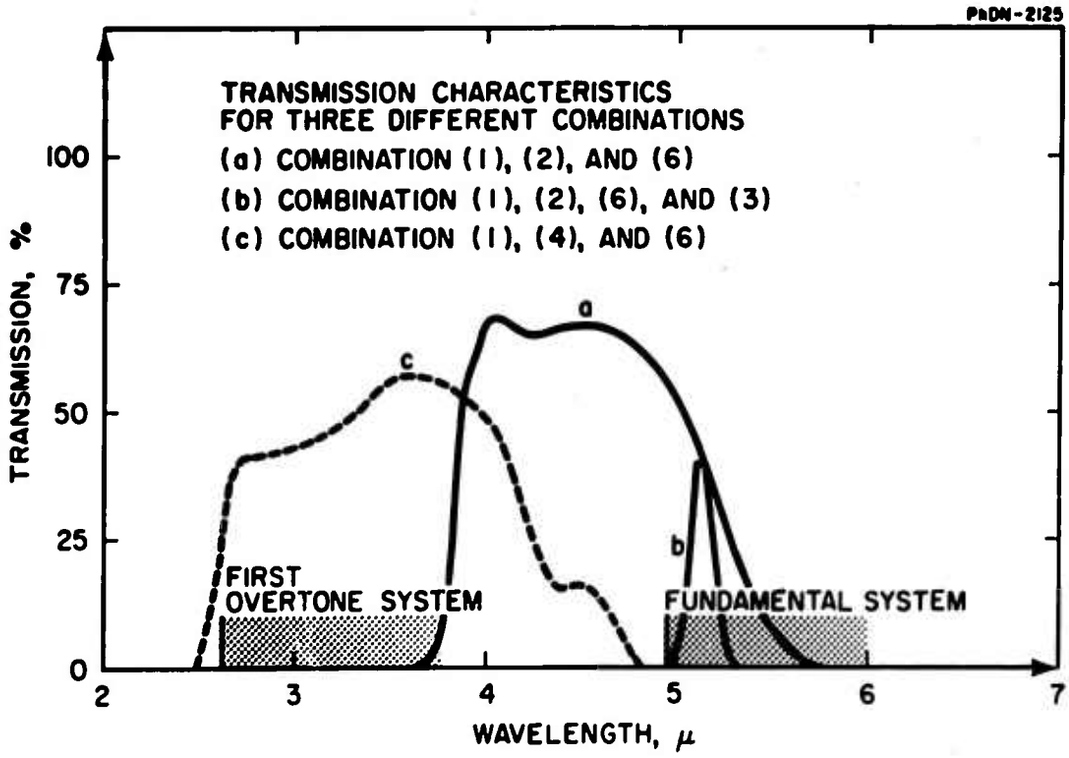

FIGURE 13 TRANSMISSION CHARACTERISTICS OF DIFFERENT COMBINATIONS

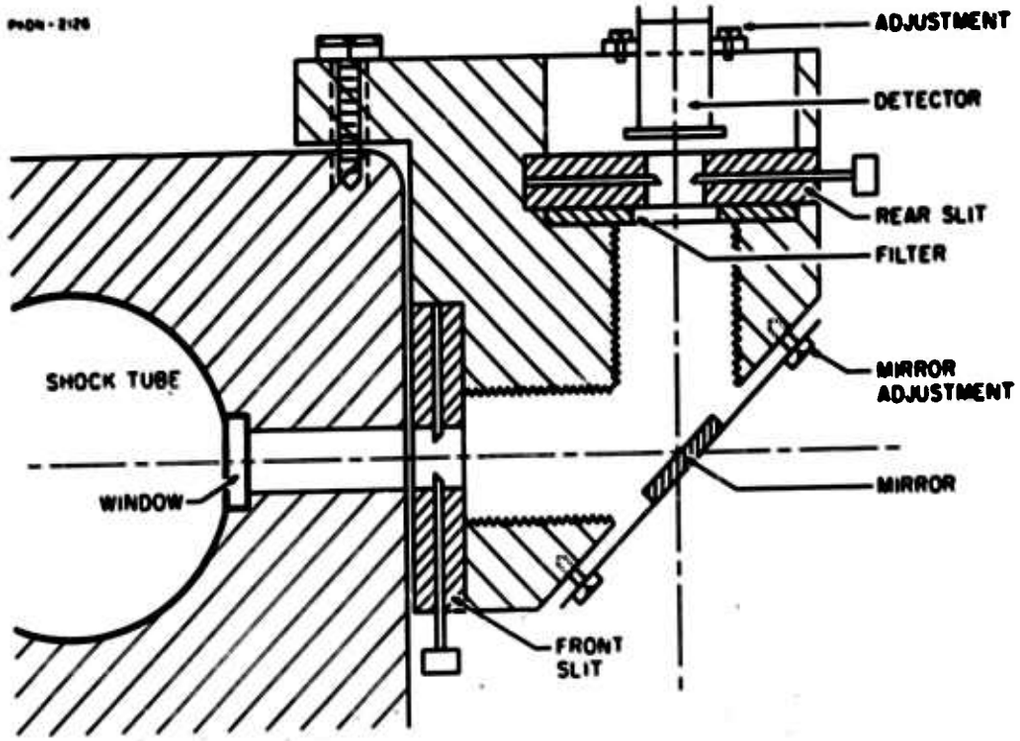

FIGURE 14 OPTICAL SYSTEM (SLIT ASSEMBLY)

PhDN - 2127

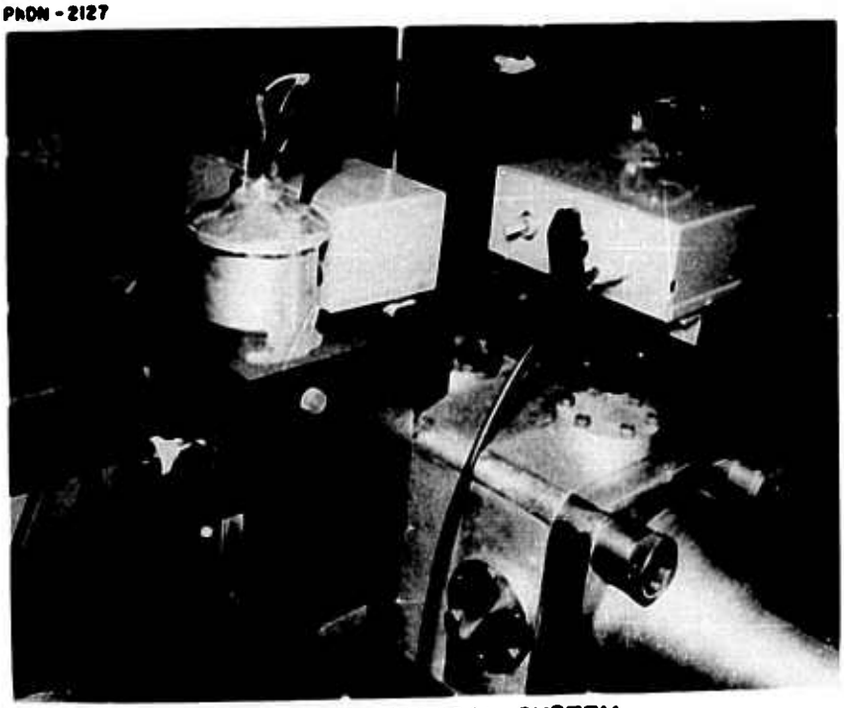

FIGURE 15 OPTICAL SYSTEM

FIGURE 16 ELECTRONIC EQUIPMENT

The rise time of the radiation signal in the laboratory system was about 5 to 6 μ sec. The signal rise depends on the shock transit time, the vibrational relaxation time of the gas, and the effective rise time of the detector and electronic equipment. An idealized mathematical treatment for the initial shape of the radiation signal is given in Appendix II. A typical example for the initial shape of the signal was computed and is shown in Figure 17. Comparison of the predicted shape with our experimental records shows good agreement within the experimental reading accuracy. The reasonably good agreement between calculated and experimentally observed initial slope of the signal seems to confirm the values for the vibrational relaxation time as given by Robben.[4] However, we are aware of the problems inherent in the interpretation of gross relaxation phenomena in terms of relaxation times.

EXPERIMENTAL RESULTS

Over 200 shock runs were made for the test series reported here. From the actual NO decomposition runs, 54 produced satisfactory reproducible data. The remaining runs were made to calibrate the velocity pickups, to check out the optical system, as well as to clean the shock tube with argon runs.

Figure 18a through j illustrates 10 of the 54 NO decomposition runs. These 10 oscillograms were selected for shock temperature steps of approximately 100°K. Of the two traces shown in each oscillogram the first represents the relative emission intensity history, the second represents the signal from the heat-transfer gauge at the window location. The oscilloscope sweep speed and the shock Mach number is given for each oscillogram. In all of our oscillograms the initial rise of the two traces coincided; therefore, we conclude that there is no appreciable reflection nor scattering in our optical system. The radiation intensity traces show, after a rise of approximately 5 μ sec, an almost constant signal level for varying time periods. This portion of the signal defines

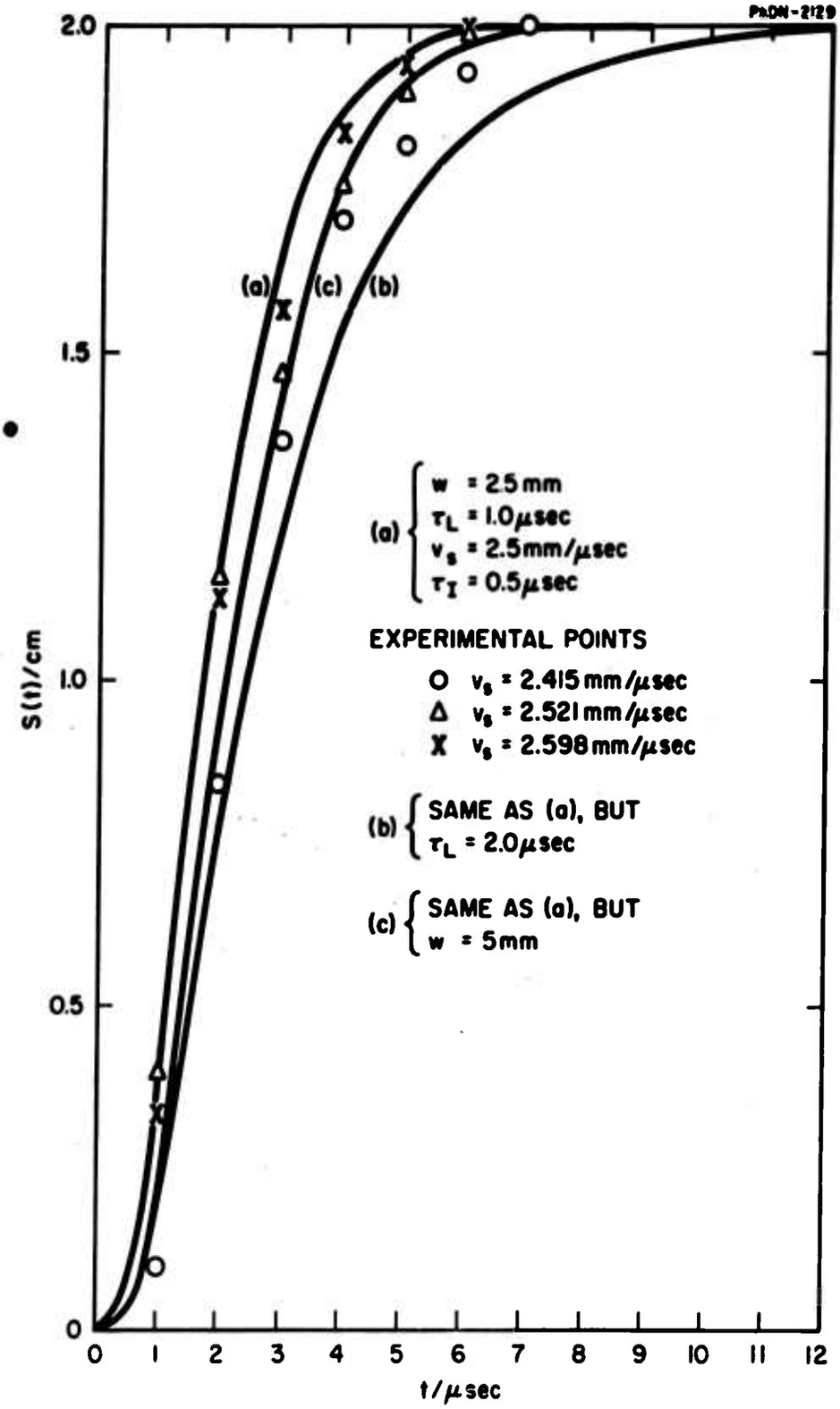

FIGURE 17 INITIAL SHAPE OF RADIATION SIGNAL

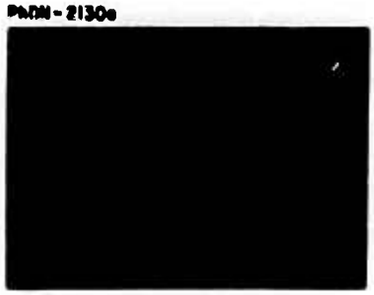

50μsec

(a)

50μsec

(b)

20μsec

(c)

20μsec

(d)

	v_s (mm/μsec)	T_s (°K)	T_e (°K)	t (μsec)	1/k* (mole μsec/cm^3)	ρ_s/ρ_o	M_s
(a)	2.066	2110	3140	255 ± 25	51.3	6.28	6.45
(b)	2.143	2250	3180	200 ± 20	42.0	6.37	6.69
(c)	2.256	2450	3240	104 ± 20	22.9	6.47	7.05
(d)	2.349	2620	3290	48 ± 5	11.0	6.55	7.34

FIGURE 18 EXPERIMENTAL DATA TRACES

PhDN-2130b

10μsec

(e)

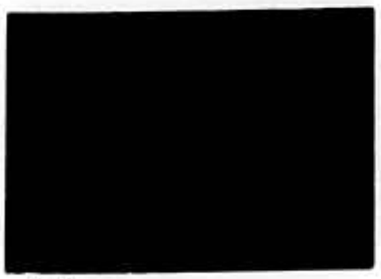

10μsec

(f)

10μsec

(g)

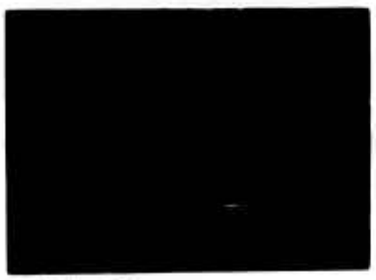

10μsec

(h)

	v_s (mm/μsec)	T_s (°K)	T_e (°K)	t (μsec)	1/k* (mole μsec/cm^3)	ρ_s/ρ_o	M_s
(e)	2.415	2745	3330	44 ± 5	10.4	6.62	7.54
(f)	2.485	2860	3370	17 ± 2	4.0	6.68	7.76
(g)	2.521	2955	3390	12 ± 1	2.9	6.71	7.87
(h)	2.559	3030	3410	13 ± 2	3.2	6.74	7.99

FIGURE 18

PhDN-2130c

10μsec

(i)

20μsec

(j)

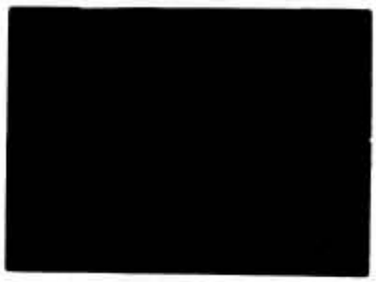

200μsec

(k)

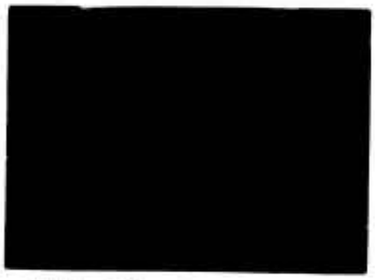

20μsec

(l)

	v_s (mm/μsec)	T_s (°K)	T_e (°K)	t (μsec)	1/k* (mole μsec/cm^3)	ρ_s/ρ_o	M_s
(i)	2.598	3110	3430	8.5 ± 1	2.1	6.78	8.11
(j)	2.679	3275	3470	6 ± 1	1.5	6.84	8.37
(k)	2.485	2860	3370	-	-	6.68	7.76
(l)	2.07	2120°					

FIGURE 18

the slow decomposition regime of NO (Regime I). After Regime I the signal level decreases rapidly to a value which is slightly higher than its "zero" value before the shock arrival. The strong temperature dependency of the duration of Regime I is apparent in Figure 18a through j. The duration varies from 250 μsec at 2110°K to 8 μsec at 3275°K (laboratory time). At the lower limit, Regime I is hardly visible because after the initial signal rise to the maximum level, the fast decomposition of NO begins almost immediately. Toward slower shock velocities, Regime I lasts almost to the maximum time available for observation. However, some of the slow shock velocity records become doubtful because of a second signal rise just before the arrival of the interface. An example of this behavior is given in Figure 18b and a tentative evaluation is given in Figure 19b. The second signal rise is also seen in Figure 18k; for this record, the sweep speed was set slow enough to observe the entire radiation history further behind the interface.

The evaluation of our traces are given in Figure 20 with temperature T_S as the abscissa and the duration of Regime I in laboratory time as the ordinate. All data points are shown with their respective error limits. The 1.5% error in velocity determination, as discussed earlier, results in a 5% uncertainty in temperature T_S. Since the low-frequency noise level of the detector and the high-frequency noise level of the electronics was very small, no additional reading uncertainty had to be included. The solid line in this graph is derived from an analysis presented previously.[3]

To represent our results independently of our particular shock conditions, an effective inverse rate coefficient $1/k^*$ is introduced in the following way:

$$1/k^* = (NO)_S/\text{mole/cc}\left(\frac{\rho_S}{\rho_O}\right) t_L/\mu\text{sec} .$$

Here $(NO)_S$ and ρ_S are the nitric oxide concentration and the density, respectively,

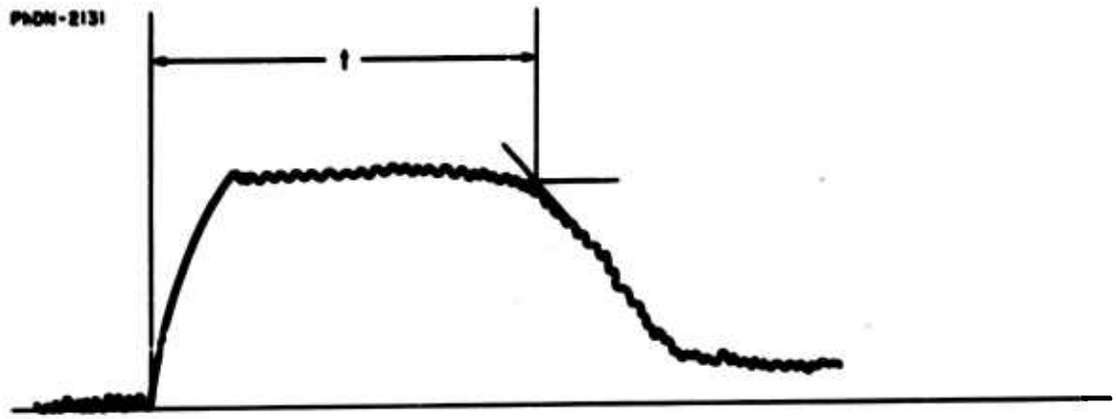

(a) UNDISTURBED BY ADDITIONAL REACTIONS

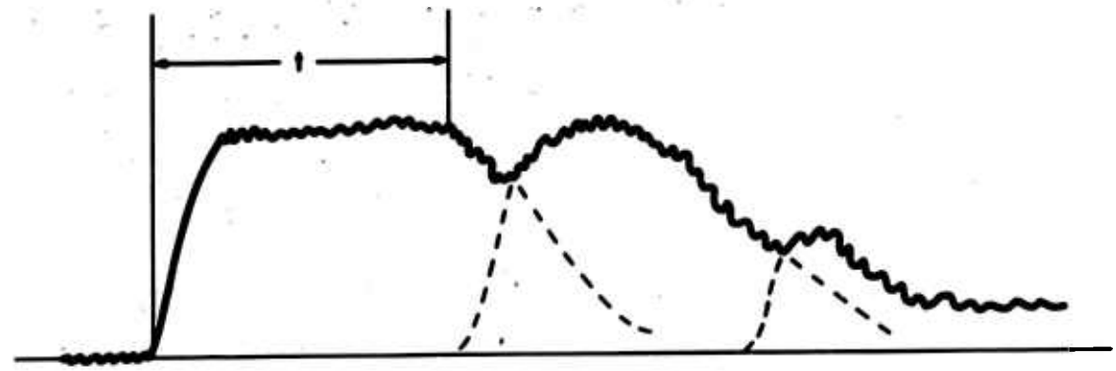

(b) DISTURBED BY ADDITIONAL REACTIONS

FIGURE 19 PLATEAU LENGTH MEASUREMENT

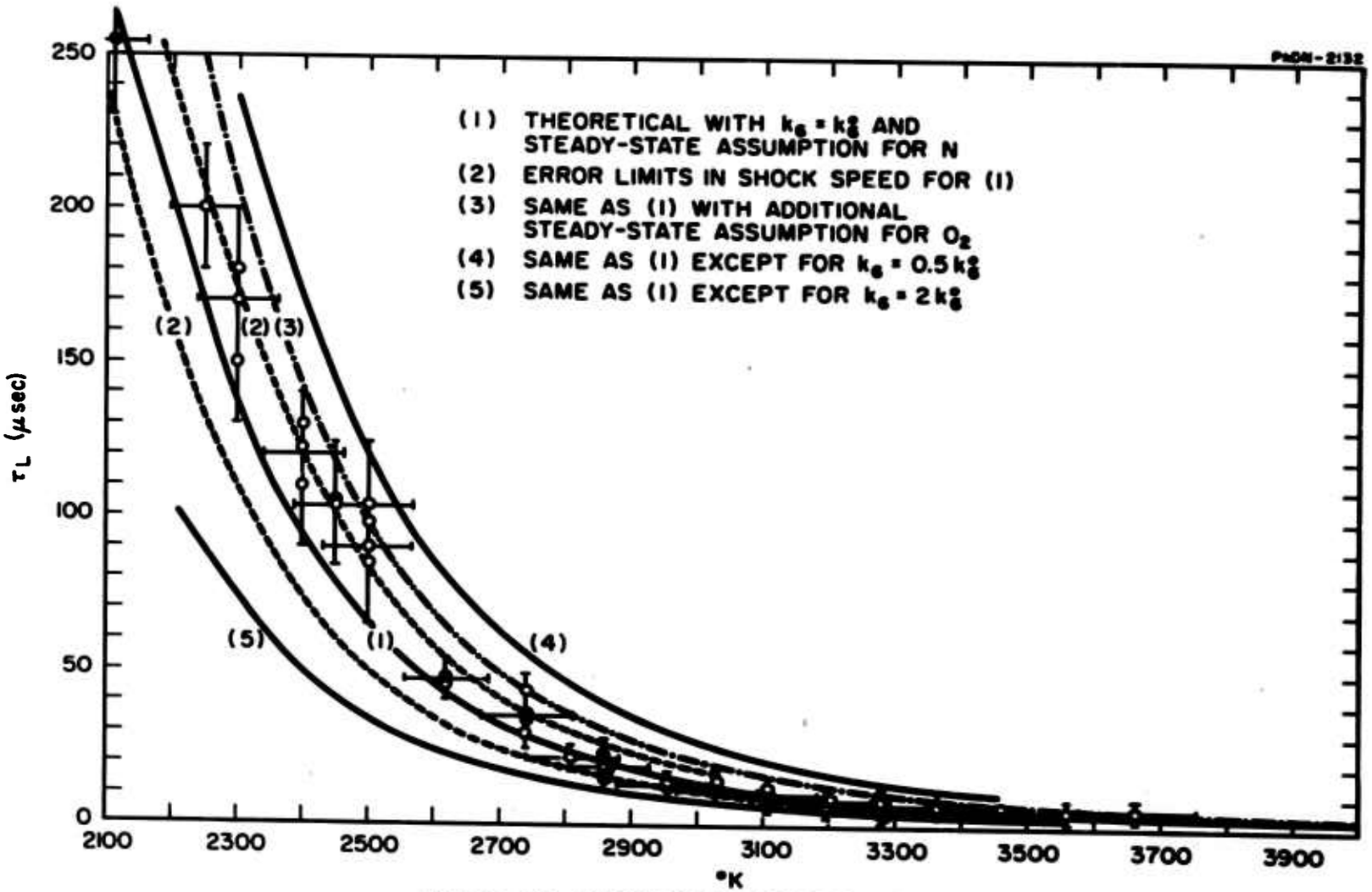

FIGURE 20 PLATEAU VS TEMPERATURE

immediately behind the shock front, ρ_o is the ambient density, and t_L is the duration of Regime I in laboratory time. A plot of $1/k^*$ versus $1/T_s$, is given in Figure 21. The data corresponding to the analytical evaluation of $1/k^*$ as outlined[3] are represented by the straight solid line. A least square curve fit of our experimental data to a linear equation of the form

$$\log 1/k^* = a_o + a_1 \frac{1}{T}$$

results in

$$1/k^* = \frac{10^{-6}}{3.1} \exp [42,400/RT] \text{ mole}/\mu\text{sec-cc} .$$

At 3450°K, the duration of Regime I is about equal to the signal rise time, therefore, this temperature represents the upper limit at which measurements are meaningful. On the other hand, the lower temperature limit for the measurements is given by 2250°K, because then Regime I extends until the arrival of the cold front. This fact is supported by a short calculation of the theoretical flow duration t (laboratory time)

$$t = \frac{(\rho_1/\rho_2)\, X}{D_s\, (1 - \rho_1/\rho_2)}$$

which leads to 530 μsec for the lower limit of our shock conditions given by $\rho_2/\rho_1 = 6.08$, $D_s = 2.143$ mm/μsec, and X = 5750 mm. As a general rule of thumb[9] for initial pressures above 5 mm Hg, the actual flow duration is one-half the ideal value given above. Therefore, in our case, the upper limit for the observation time is about 265 μsec. The data point at 2110°K shown in Figures 20 and 21 is questionable as a result of the above consideration.

Since we were interested in the time duration of the slow NO decomposition regime only in the data evaluation, the time lapse between the initial signal

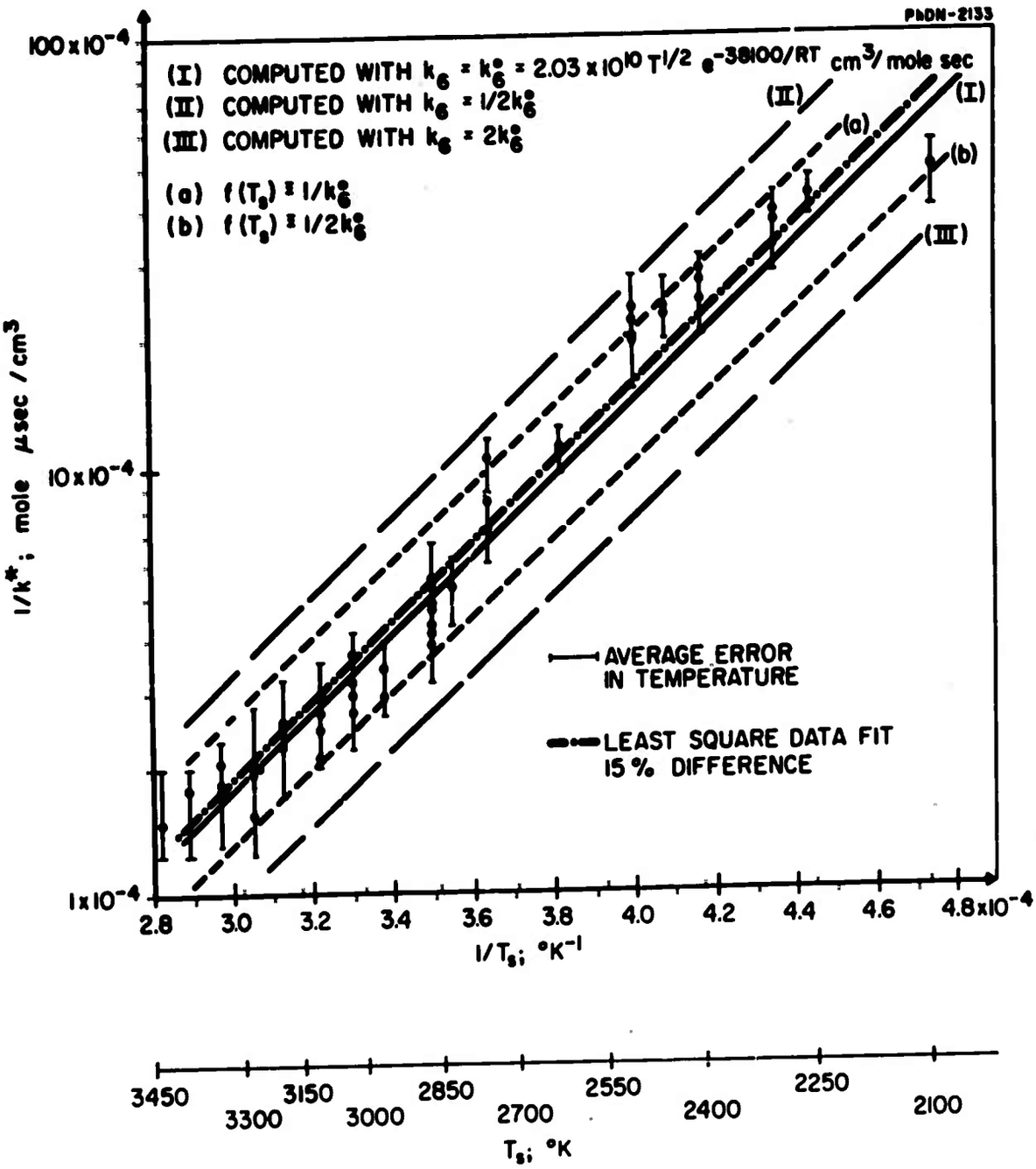

FIGURE 21 CHARACTERISTIC TIME PARAMETER $1/k^*$ AS A FUNCTION OF SHOCK VELOCITY

rise and the transition from the slow to the fast decomposition was determined. Because this transition is rather gradual the determination of the duration can only be made within a ±10% error (Figure 19a). In some cases, the fast decomposition regime is obscured by signal fluctuations (Figure 18c); the reading accuracy is lowered to ± 20%. The deviation of the experimental data from the theoretical curve is about 15% to higher values of $1/k^*$; the experimental data as a function of temperature show also a slightly different slope than the theoretical curve. The mean deviation of the experimental data from the least mean square fitted is 16.3%.

In Figure 18 ℓ a record of a reflected shock wave through NO is shown. The detector as well as the heat-transfer gauge were located 29 mm from the end plate. It is found that the radiation signal and the signal from the heat-transfer gauge do not coincide for the reflected shock, whereas they do for the incident shock. This fact seems to indicate that the reflected shock interacts with the boundary layer and produces a bifurcation of the Mach line. Therefore, no further attempts have been made to measure the NO decomposition history behind the reflected shock wave.

ACKNOWLEDGMENT

It is a pleasure to thank S. S. Penner and R. Duff for many helpful suggestions. Thanks are also extended to F. Vogler, who designed and built the optical slit system, to S. Trujillo, who advised us in the electronic circuitry and to C. Sabin and N. Hankin who designed and built the shock tube.

REFERENCES

1. E. Freedman, J. Daiber, and W. H. Wurster, Bull. Am. Phys. Soc. II, 5, 134 (1960).

2. J. J. Allport, Bull. Am. Phys. Soc. II, 5, 250 (1960).

3. K. P. G. Sulzmann, C. B. Ludwig, General Dynamics Report, ZPh-087, "Duration of the Slow NO Decomposition Regime behind Shock Waves Around 3000°K and Its Relation to the Rate Coefficient of the Exchange Path $NO + O \rightarrow N + O_2$," March 1, 1961.

4. F. Robben, J. Chem. Phys. 31, 420 (1959).

5. F. R. Gilmore, "Equilibrium Composition and Thermodynamic Properties to Air to 24,000°K," RAND Corporation, RM 1543 (1955).

6. R. E. Duff, N. Davidson, J. Chem. Phys. 31, 1018 (1959).

7. K. L. Wray, T. D. Teare, "Kinetic Studies of Nitric Oxide," AVCO Research Note, 134 (1959).

8. N. N. Hankin, ZPh-013, General Dynamics/Convair Physics Section Progress Report "The Shock Tube Laboratory," p. 215 (1958).

9. A. Roshko, Phys. Fluids 3, 835 (1960).

10. K. G. P. Sulzmann, C. B. Ludwig, General Dynamics/Convair Physics Section Internal Memorandum, Ph-200-M, "Observable Spectrally Emitted Intensities behind Incident and Reflected Shock Wave," May 1, 1961.

APPENDIX I

DETERMINATION OF THE LOAD RESISTOR FOR THE HEAT TRANSFER GAUGE

The arrangement for the heat-transfer gauge circuitry was as follows:

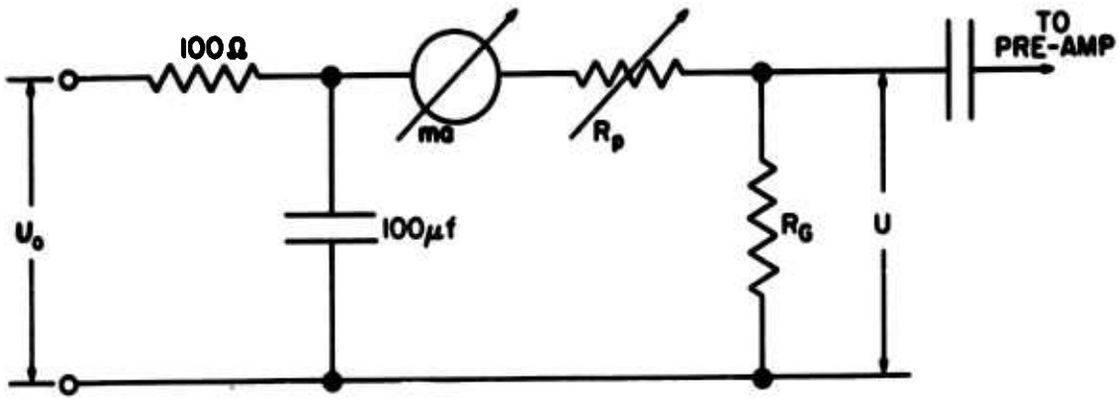

The voltage U across the gauge is represented by $U = IR_G = R_G U_o (R_G + R_p)^{-1}$. An increase ΔR of the resistance in the gauge results in an increase ΔU of the voltage given by

$$U + \Delta U = (I + \Delta I)(R_G + \Delta R) = \frac{R_G + \Delta R}{R_p + R_G + \Delta R} U_o$$

The maximum of ΔU is found from

$$\frac{d\left(\frac{\Delta U}{U_o}\right)}{d R_p} = - \frac{R_G + \Delta R}{(R_p + R_G + \Delta R)^2} + \frac{R_G}{(R_p + R_G)^2} = 0$$

for a potentiometer resistance R_p given by

$$R_p = R_G \sqrt{1 + \left(\frac{\Delta R}{R_G}\right)^2} .$$

Therefore, because $\Delta R \ll R_G$, the optimum potentiometer setting is $R_p = R_G$.

APPENDIX II

INITIAL SHAPE OF RADIATION SIGNAL

To estimate the initial slope of the radiation signal as observed at the oscilloscope we use the approach as outlined. We assume that the vibrational relaxation of the gas behind the shock wave occurs uniformly in planes perpendicular to the direction of the shock wave propagation. Making the strongly idealizing assumption, that the vibrational relaxation in first order approximation is governed by a single relaxation time τ_p, the partial pressure p of the molecules in the upper vibrational state at the time t_p after shock arrival may be approximated by [10]

$$p/p_o = 1 - e^{-t_p/\tau_p} \ . \tag{1}$$

Here, p_o is the partial pressure of the radiators in the upper vibrational level after complete vibrational relaxation, and t_p is the particle time behind the incident shock wave. For transparent gases the radiation intensity in the spectral interval $\nu + d\nu$ emerging through a small slit of finite width w and height h into a small solid angle $d\Omega$ subtended by the receiver may be approximated by [10]

$$I_\nu \, d\nu = R_\nu^o \, P_\nu \, p_o \, \ell \, h \, \frac{d\Omega}{\pi} \, d\nu \, x$$

$$x \begin{cases} v_s \tau_L \left\{ \frac{t}{\tau_L} - \left[1 - \exp\left(- \frac{t}{\tau_L} \right) \right] \right\}, & \text{for } o \leq t \leq \frac{w}{v_s} , \\ w - v_s \tau_L \left[\exp\left(\frac{w}{v_s \tau_L} \right) - 1 \right] \exp\left(- \frac{t}{\tau_L} \right), & \text{for } t \geq \frac{w}{v_s} , \end{cases} \tag{2}$$

where

R_ν^o = spectral blackbody radiancy,

P_ν = spectral absorption coefficient,

ℓ = effective geometrical depth of the gas layer,

v_s = shock velocity, and

$\tau_L = \frac{\rho_o}{\rho} \tau_p$ = vibrational relaxation time as observed in the laboratory system.

The laboratory time t in Equation (2) is counted from the instant of the shock front arrival at the front edge of the slit. If the above signal is fed into a detector-amplifier system with an over-all effective instrumental relaxation time τ_I and an amplification factor B_ν, the recorded signal becomes after integrating over the observed spectral interval (ν_1, ν_2)

$$S(t) = \int_{\nu_1}^{\nu_2} d\nu \int_{-\infty}^{t} T_\nu (t-t') I_\nu(t')dt' . \qquad (3)$$

Here,

$$T_\nu(z) = \frac{B_\nu}{\tau_I} \exp\left(-\frac{z}{\tau_I}\right) \qquad (4)$$

is the detector-amplifier response function. The factor B_ν in the function $T_\nu(z)$ includes, besides the frequency response of the detector, the transmission characteristics of filters which are placed in front of the detector. Here the assumption has been made that the combined detector-amplifier response time is independent of the radiation frequency in the spectral interval observed. Hence, integration over the observed spectral interval in Equation (3), in view of

Equation (2), results in

$$S(t) = \frac{A}{\tau_I} \int_{-\infty}^{t} f(t') \exp\left(-\frac{t-t'}{\tau_I}\right) dt' \qquad (5)$$

where

$$f(t) = 0, \qquad \text{for } t \leq 0,$$

$$f(t) = v_s \tau_L \left\{ \frac{t}{\tau_L} - \left[1 - \exp\left(-\frac{t}{\tau_L}\right)\right] \right\}, \qquad \text{for } 0 \leq t \leq \frac{w}{v_s},$$

$$f(t) = w - v_s \tau_L \left[\exp\left(\frac{w}{v_s \tau_L}\right) - 1 \right] \exp\left(-\frac{t}{\tau_L}\right), \quad \text{for } t \geq \frac{w}{v_s}.$$

Here, the quantity

$$A = \int_{\nu_1}^{\nu_2} d\nu \; B_\nu \; R_\nu^o \; P_\nu \; p_o \; \ell h \frac{d\Omega}{\pi} \qquad (6)$$

is still a function of the temperature of the gas and depends on the geometry, filter-detector spectral characteristic, and the geometry of the slit-detector arrangement.

For $\tau_L \neq \tau_I$, which is satisfied for our particular instrumental arrangement, and for practically constant A, integration of Equation (5), results in the following expressions for the signal S as observed at the oscilloscope:

$$S(t) \quad 0 \leq t \leq \frac{w}{v_s} = A \left\{ v_s t - v_s \tau_L \frac{\tau_L}{\tau_L - \tau_I} \left[1 - \exp\left(-\frac{t}{\tau_L}\right)\right] + v_s \tau_I \frac{\tau_I}{\tau_L - \tau_I} \left[1 - \exp\left(-\frac{t}{\tau_I}\right)\right] \right\}, \qquad (7a)$$

and

$$S(t) = A\left\{ w - v_s \tau_L \frac{\tau_L}{\tau_L - \tau_I}\left[1 - \exp\left(-\frac{w}{v_s \tau_L}\right)\right]\exp\left[-\frac{1}{\tau_L}\left(t - \frac{w}{v_s}\right)\right] \right.$$

$$t \geq \frac{w}{v_s}$$

$$\left. + v_s \tau_I \frac{\tau_I}{\tau_L - \tau_I}\left[1 - \exp\left(-\frac{w}{v_s \tau_I}\right)\right]\exp\left[-\frac{1}{\tau_I}\left(t - \frac{w}{v_s}\right)\right]\right\} . \qquad (7b)$$

From the above expressions it is evident that the signal starts with zero initial slope and approaches rapidly a linear increase for $w/v_s \geq \tau_L, \tau_I$. The signal exhibits a point of inflection for $t = w/v_s$ after which it approaches its final magnitude exponentially.

For comparison of the initial signal shape, as predicted from the very simplified treatment outlined above, with the experimentally observed signal shape the following experimental situation is considered. A shock wave travels with a velocity $v_s = 2.5$ mm/μsec into NO at an ambient pressure $P_a = 10$ mm Hg and at an ambient temperature $T_a = 300°K$. The vibrational relaxation time τ_L for these conditions can be estimated from the data[4] to be about 1μsec. The effective instrumental response time in our experiments has been determined to be at most 0.5 μsec. The calculated and experimentally obtained initial signal for these conditions and a slit width of 2.5 mm is given in Figure (17), curve (a). In this figure the oscilloscope signal S(t) has been normalized in such a way that after vibrational relaxation the signal level becomes 2 cm on the oscilloscope screen. The signal approaches 99% of its vibrational equilibrium level after about 6 μsec; this agrees very well with our experimental observations. In the same figure, the results for a change of the vibrational relaxation time to $\tau_L = 2\mu$sec, ourve (b), and for a change of the slit width to w = 5 mm, curve (c), respectively, are included. Comparison of the three curves (a), (b), and (c)

shows that the initial slope of the signal is more sensitive to changes of the vibrational relaxation time τ_L than to changes of the slit width w. The reasonably good agreement (within the experimental scatter and within the limitations of the simplified treatment) between the experimental data and curves (a) and (b) seems to confirm the value used for τ_L. This value is based on the experimental data given by Robben.[4]